HHS Public Access

Author manuscript

Cancer Discov. Author manuscript; available in PMC 2016 January 01.

Published in final edited form as:

Cancer Discov. 2015 July ; 5(7): 752–767. doi:10.1158/2159-8290.CD-14-0849.

ARID1A Deficiency Impairs the DNA Damage Checkpoint and Sensitizes Cells to PARP Inhibitors

Jianfeng Shen[1], **Yang Peng**[2], **Leizhen Wei**[3,4], **Wei Zhang**[1], **Lin Yang**[1,5], **Li Lan**[3,4], **Prabodh Kapoor**[6], **Zhenlin Ju**[7], **Qianxing Mo**[8], **Ie-Ming Shih**[9], **Ivan P. Uray**[1], **Xiangwei Wu**[1], **Powel H. Brown**[1], **Xuetong Shen**[6], **Gordon B. Mills**[2], and **Guang Peng**[1,*]

[1]Department of Clinical Cancer Prevention, The University of Texas MD Anderson Cancer Center, Houston, Texas 77030, USA

[2]Department of Systems Biology, The University of Texas MD Anderson Cancer Center, Houston, Texas 77054, USA

[3]Department of Microbiology and Molecular Genetics, The University of Pittsburgh School of Medicine, Pittsburgh, PA 15213, USA

[4] University of Pittsburgh Cancer Institute, Pittsburgh, PA 15232, USA

[5]Department of Medical Oncology, Tongji Hospital, Tongji Medical College, The University of Huazhong Science & Technology, Wuhan, Hubei Province 430022, P.R. China

[6]Department of Epigenetics and Molecular Carcinogenesis, The University of Texas MD Anderson Cancer Center, Houston, Texas 77030, USA

[7]Department of Bioinformatics and Computational Biology, The University of Texas MD Anderson Cancer Center, Houston, Texas 77030, USA

[8]Division of Biostatistics, Dan L. Duncan Cancer Center, Baylor College of Medicine, Houston, TX 77030, USA

[9]Department of Pathology, Johns Hopkins Medical Institutions, Baltimore, MD 21287, USA

Abstract

ARID1A, a chromatin remodeler of the SWI/SNF family, is a recently identified tumor suppressor that is mutated in a broad spectrum of human cancers. Thus, it is of fundamental clinical importance to understand its molecular functions and determine whether ARID1A deficiency can be exploited therapeutically. In this manuscript, we report a key function of ARID1A in regulating the DNA damage checkpoint. ARID1A is recruited to DNA double strand breaks (DSBs) via its interaction with the upstream DNA damage checkpoint kinase ATR. At the molecular level, ARID1A facilitates efficient processing of DSB to single strand ends, and sustains DNA damage signaling. Importantly, ARID1A deficiency sensitizes cancer cells to PARP inhibitors in vitro and in vivo providing a potential therapeutic strategy for patients with ARID1A-mutant tumors.

[*]**Correspondence:** Peng, G., Department of Clinical Cancer Prevention, Unit 1360, The University of Texas MD Anderson Cancer Center, Houston, TX 77054, USA; Tel: +1 713 834 6151; Fax: +1 713 834 6397; gpeng@mdanderson.org..

DISCLOSURE OF POTENTIAL CONFLICTS OF INTEREST

No potential conflicts of interest were disclosed by the other authors.

INTRODUCTION

ARID1A (the AT-rich interactive domain 1A gene) has been identified as one of the most frequently mutated genes in human cancers by multiple next-generation genomic sequencing studies (1-3). *ARID1A* mutation rates ranging from 10% to 57% have been identified across multiple tumor lineages, including ovarian clear cell carcinoma, uterine endometrioid carcinoma, gastric cancer, hepatocellular carcinoma, esophageal adenocarcinoma, breast cancer, pancreatic cancer, transitional-cell carcinoma of the bladder, renal cancer, Waldenström macroglobulinemia, pediatric Burkitts lymphoma, and cholangiocarcinoma (1-3). ARID1A, also known as BAF250a, is a subunit of the evolutionarily conserved SWI/SNF chromatin remodeling complex (4, 5). The SWI/SNF complex repositions, ejects, or exchanges nucleosomes, which modulate DNA accessibility to cellular processes involved in chromatin structure, such as transcription, DNA replication, and DNA repair (6-8). However, how ARID1A deficiency contributes to cancer development and approaches to exploit ARID1A deficiency therapeutically are not known.

ATR is a member of the phosphatidylinositol 3-kinase-like kinase family. Along with another kinase, ataxia telangiectasia-mutated (ATM), ATR functions as a central regulator controlling cellular responses to DNA damage (9-11). In general, ATM is activated by double-strand DNA breaks (DSBs), whereas ATR responds to single-strand DNA breaks (SSBs) (12). However, the ATM- and ATR-activating DNA lesions are interconvertible: DSBs activate ATM but can also activate ATR as a consequence of DSB end resection, which generates a single-stranded region (13-15). Unlike ATM, ATR is essential for cell survival (16), supporting the functional importance of ATR for genome maintenance programs. For example, in S phase, ATR regulates replication initiation, replisome stability, and replication fork restart (17). In G2 phase, ATR prevents premature mitotic entry in the presence of damaged DNA via the G2 checkpoint (18, 19). Thus, a key question remains unanswered: how is ATR signaling regulated allowing it to perform versatile roles in DNA damage response (DDR)? One possibility is that ATR-interacting proteins fine-tune the temporal and spatial functions of ATR in DDR. Therefore, we conducted a proteomic analysis to systematically identify ATR-interacting proteins. In addition to many known ATR-binding proteins, such as ATRIP, we identified ARID1A as an unexpected interacting partner of ATR. Human cancers result in large part from the accumulation of multiple genetic alterations, including mutations, deletions, translocations, and amplifications (20). Thus, our proteomic result raised the intriguing question of whether ARID1A, through its interaction with ATR, plays a role in maintaining genomic integrity that could be exploited as a therapeutic liability.

In this study, we found that ARID1A is recruited to DSBs via its interaction with ATR. In response to DNA damage, ARID1A facilitates DNA DSB end processing to generate RPA-coated single-strand DNA (ssDNA), and sustains ATR activation in response to DSBs. Loss of ARID1A leads to impaired checkpoint activation and repair of DNA DSBs, which sensitizes cells to DSB-inducing treatments, such as radiation and poly(ADP-ribose) polymerase (PARP) inhibitors. Thus, our results provide biological insights into the function

ARID1A as a tumor suppressor in human cancers and a mechanistic basis for targeting ARID1A-deficient tumors.

RESULTS

ARID1A is Recruited to DNA Breaks via Its Interaction with ATR

To explore the mechanisms regulating the functions of ATR in DDR, we conducted an immunoprecipitation (IP) assay to enrich ATR-associated protein complexes which were then subjected to silver staining and mass spectrometry (Fig. 1A). In addition to known ATR-binding proteins, such as ATRIP, we identified ARID1A as a binding partner of ATR (Fig. 1A and Supplementary Fig. 1). Notably, in addition to ARID1A, multiple subunits of the SWI/SNF complex including BRG1, BAF57, BAF60, BAF170 and SNF5 were also identified by the mass spectrometry analysis, suggesting that ATR interacts broadly with the SWI/SNF complex. To confirm the interaction between ARID1A and ATR, we performed reciprocal IP with V5-tagged ARID1A (Fig. 1B) and endogenous IP analyses (Fig. 1C and Supplementary Fig. 2), which confirmed that ARID1A interacts with ATR. Given the important role of ATR in DDR, next we tested whether ARID1A is recruited to DNA breaks. We used chromatin IP (ChIP) assay to examine whether ARID1A was recruited to the proximity of a single site-specific I-*Sce*I-induced DSB (Fig. 1D and Supplementary Fig. 3A), as previously described (21, 22). Interestingly, we found that ARID1A was enriched at the chromatin region close to this DSB (Fig. 1D and Supplementary Fig. 3B, 3C). To facilitate visualization of the recruitment of ARID1A to DNA lesions, we used a light activation system (KillerRed System) (23) to determine whether ARID1A localized at sites of DNA damage. Briefly, KillerRed (KR) is a light-stimulated ROS inducer fused to a tet-repressor (tetR) or TA (transcription activator; tetR+VP16), which bind to a TRE cassette (~ 90 kb) integrated at a defined genomic locus in U2OS cells (U2OS TRE cell line)(24). KR facilitates the formation of oxygen radicals and superoxide through the excited chromophore (25, 26) to induce DNA damage including single strand and DSBs. Targeting the expression of KR to one specific genome site allows visualization of the recruitment of specific proteins to a site of DNA damage. As shown in Fig. 1E and Supplementary Fig. 4, EGFP-tagged ARID1A predominantly localized in the nucleus. Upon activation of KillerRed, ARID1A showed a specific enrichment at the DNA damage site, which co-localized with TA-KR focus but not with TA-mcherry, indicating the recruitment of ARID1A at TA-KR is specific to DNA damage. These findings revealed that ARID1A interacts with ATR and is recruited to DSBs.

We next set out to determine whether the recruitment of ARID1A to DSBs is dependent on its interaction with ATR. First, we transiently knocked down ATR and examined the recruitment of ARID1A to DSBs via I-*Sce*I-based ChIP. As shown in Fig. 1F, in ATR knockdown cells, recruitment of ARID1A to DSBs was significantly reduced. This suggested that ATR is required for recruiting ARID1A to DNA lesions. Second, we examined whether the DNA damage signaling induced by ATM and ATR is required for recruitment of ARID1A to DSBs. We treated cells with chemical inhibitors of ATM or ATR. These inhibitors effectively blocked DNA damage signaling as shown by their impact on phosphorylation of ATM and CHK1 (Fig. 1G). The ATM inhibitor markedly decreased

the recruitment of ARID1A to DSBs (Fig. 1G). The ATR inhibitor also decreased recruitment of ARID1A to DSBs, but to a lesser extent, whereas ATR knockdown significantly reduced the recruitment of ARID1A to DSBs (Fig. 1F, G). Consistent with previous findings that ATR recruitment to DSBs requires ATM and not the converse (13-15), these data suggested that interaction between ARID1A and ATR, with ATR acting as a scaffold, and DNA damage signaling initiated by ATM are required for efficient ARID1A recruitment to DSBs.

To understand the molecular details of ARID1A-ATR interaction and the recruitment of ARID1A to DSBs, we first used two deletion constructs to test whether ARID1A binds to ATR through its N-terminal or C-terminal half. As shown in Fig. 1H, binding of ATR to the C-terminal of ARID1A was readily detectable, whereas N-terminal ARID1A did not pull down ATR even though the N-terminal ARID1A expressed at levels similar to the full-length protein. This result suggested that the domains required for ATR interaction are located in the C-terminal half of ARID1A. Next, we generated deletion mutants of ARID1A to further map the regions mediating its interaction with ATR (Fig. 1I-K). Using these constructs, we found that regions from 1800-1900 amino acids (aa) and 2100-2200 aa at the C-terminal half of ARID1A were essential for its interaction with ATR (Fig. 1I, J). We further examined the recruitment of deletion mutants to DSBs. Indeed, we found that deletion of ARID1A-interacting domain suppressed the recruitment of ARID1A to DSBs (Fig. 1L and Supplementary Fig. 5).

Collectively, these data showed that ARID1A interacts with ATR via its C-terminal region, which mediates its recruitment to DSBs.

ARID1A Is Required for Proper G2/M DNA Damage Checkpoint

Next, we tested whether ARID1A deficiency impairs cellular response to DNA damage. As our model system, we used isogenic HCT116 cell lines with wild-type ARID1A and a knock-in mutant ARID1A (Q456*/Q456*) that abolishes ARID1A expression because of an early stop codon. We first examined cell cycle distribution at different time points after exposure to IR. As shown in Fig. 2A, 1 h after irradiation, control cells started to accumulate at the G2/M checkpoint. At 4 h and 8 h after irradiation, there was a significant increase of cells at G2/M phase, suggesting that ARID1A-depleted cells have weakened G2/M checkpoint activation. Sixteen hours after irradiation, while control cells still had a large proportion of cells arrested at the G2/M checkpoint, ARID1A-depleted cells exhibited a markedly reduced proportion of cells at the G2/M checkpoint and a significant increase of cells in G1 phase (Fig. 2A). These results indicated that ARID1A deficiency leads to impaired G2/M checkpoint initiation and maintenance. To confirm these results, we used phospho-Histone H3 staining to measure the fraction of mitotic cells after exposure to IR in ARID1A-depleted cells. Without IR treatment, there was no apparent difference in the percentage of mitotic cells between control and ARID1A-depleted cells (Fig. 2B). After exposure to IR, in control cells, the percentage of mitotic cells was significantly reduced and started to recover 16 h after IR (Fig. 2B). In contrast, ARID1A-deficient cells showed a slower decrease in numbers of mitotic cells at early time points after IR exposure and a significantly increased percentage of cells re-entering mitosis at 16 h after IR, suggesting

defective G2/M checkpoint initiation and maintenance (Fig. 2B). In accord with this finding, as shown in Fig. 2C, ARID1A depletion led to a marked increase in cumulative mitotic reentry after IR exposure revealed by paclitaxel treatment, which blocks mitotic exit. Defective G2/M checkpoint maintenance was not due to a differential response to paclitaxel between control and ARID1A-null cells, since we observed a similar block in mitotic accumulation in cells not treated with IR (Fig. 2C). ARID1A expression was effectively depleted in ARID1A-null cells (Fig. 2D). These data are consistent with ARID1A deficiency significantly impairing G2/M checkpoint initiation and maintenance.

As ARID1A is a subunit of the SWI/SNF complex, we next asked whether the chromatin remodeling activity of SWI/SNF is required for G2/M checkpoint response. We knocked down the core catalytic subunits BRG1 or BRM in U2OS cells (Supplementary Fig. 6) and found that BRG1 deficiency led to an increase of mitotic cells 16 h after exposure to IR, similar to the increase observed in ARID1A-null cells (Fig. 2E). This result suggested that ARID1A-associated BRG1-SWI/SNF is required for maintaining G2/M cell cycle arrest after induction of DSBs.

ARID1A Deficiency Impairs DSB-Induced ATR Activation

Having observed a defective DNA damage checkpoint in ARID1A-deficient cells, we further examined whether ARID1A deficiency impairs the DNA damage checkpoint signaling pathway. We treated cells with IR and examined the activation of CHK1, a key G2/M checkpoint regulator. In ARID1A-depleted cells, we found reduced CHK1 (S317) phosphorylation in response to IR, particularly at 8 h after IR (Fig. 3A). In response to DSBs, CHK1 (S317) can be phosphorylated by either ATM or ATR. Thus, we examined whether ARID1A deficiency affected ATM and/or ATR activation. In response to DNA damage, ATM (S1981) and ATR (T1989) undergo autophosphorylation, which provides a surrogate marker for kinase activation (13, 27-29). ARID1A depletion remarkably reduced ATR activation (phosphorylation of ATR (T1989)) in response to IR (Fig. 3B), but did not alter ATM activation (phosphorylation of ATM (S1981)) or recruitment of ATM to DNA damage sites (Fig. 3C and Supplementary Fig. 7). Previous studies showed that the G2/M checkpoint is impaired in the absence of ATR (16). Thus, our data are consistent with ARID1A depletion impairing ATR activation in response to DSBs and thereby altering checkpoint signaling.

In general, DSB ends are the preferred substrate for ATM binding, which activates first ATM and then ATR to sustain ATM-initiated signaling (11). It has been shown that phosphorylation of H2AX in response to IR is mediated by both ATM and ATR (30, 31). Therefore, we examined the effect of ARID1A deficiency on the dynamics of H2AX phosphorylation. As we expected, chromatin binding of γ-H2AX was significantly reduced in ARID1A deficient cells at 8 h compared to 4 h after IR, indicating impairment of sustained γ-H2AX foci formation (Fig. 3D). To confirm this result, we tested whether ARID1A deficiency reduced γ-H2AX foci formation, which directly reflects the accumulation of γ-H2AX at DSBs. As shown in Fig. 3E, γ-H2AX foci formation was significantly reduced at later time points after IR. In addition, we examined the foci formation by DNA damage-responsive protein 53BP1, a key adaptor protein in checkpoint

response whose recruitment to DSBs is dependent on the protein platform assembled by γ-H2AX formation (32). Consistent with the reduced γ-H2AX foci formation at 8 h after exposure to IR, 53BP1 foci formation was remarkably reduced in ARID1A deficient cells (Fig. 3F). As shown in Supplementary Fig. 8A, we used a comet assay to determine the presence of DSBs. Control and ARID1A-depleted cells had similar levels of DSB formation 8 h after exposure to IR, suggesting that reduced γ-H2AX and 53BP1 foci formation was not due to a reduced level of DSBs. Collectively, these results indicated that ARID1A deficiency impairs ATR-mediated signaling in response to DSBs, which is required for sustaining DSB-induced DNA damage signaling.

ARID1A Deficiency Impairs DSB End Resection and Thereby Impairs DSB-induced ATR Signaling

Next, we sought to determine the molecular mechanism underlying the defective DSB-induced ATR activation in ARID1A-deficient cells. In response to DSBs, ATM is directly activated by the MRN (MRE11-RAD50-NBS1) complex, which is required to recruit ATM to DSBs (33-35), whereas ATR activation and recruitment to DSBs requires the formation of RPA-coated SSBs, which arise from 5'-3' resection of DSB ends (18, 36). Therefore, we asked whether ARID1A depletion affects the process of DSB end resection, leading to reduced efficiency of ATR activation.

First, we examined phosphorylation of the ssDNA-binding protein RPA in ARID1A-depleted cells as an indicator of DSB resection efficiency (37). As shown by Western blotting (Fig. 4A), IR-induced phosphorylation of the RPA2 subunit (Ser4 and Ser8) was significantly reduced after ARID1A depletion. In contrast, ARID1A deficiency did not affect RPA phosphorylation in response to replication stress stimuli hydroxyuridine (HU) and ultraviolet light (UV) even though both HU and UV induce much stronger RPA phosphorylation than IR (Fig. 4B). This result suggested that ARID1A specifically affects DSB-induced formation of ssDNA. To confirm this observation, we used immunofluorescent staining to detect RPA phosphorylation at DNA damage sites. Notably, ARID1A depletion markedly reduced p-RPA (Ser4/Ser8) foci formation, consistent with decreased RPA accumulation and impaired ssDNA formation at DSBs (Fig. 4C and Supplementary Fig. 8B). We also tested the effect of ARID1A loss on the chromatin environment around DSBs by examining histone H3 occupancy at I-*Sce*I-induced DSBs by ChIP assay. We found that H3 deposition was not altered in ARID1A-depleted cells before DNA damage (Fig. 4D). However, H3 occupancy was much higher in ARID1A-depleted than control cells after induction of DSBs by I-*Sce*I. These data supported impaired DSB end resection due to loss of ARID1A, suggesting that recruitment of ARID1A to DSB is required to create a favorable chromatin environment for efficient DSB end resection. Next, we determined whether ARID1A depletion affects DSB repair via homologous recombination (HR) or single-strand annealing (SSA), which are the repair mechanisms requiring DSB end resection (Supplementary Fig. 9). In line with our finding that ARID1A is required for efficient DSB end resection, we found that ARID1A knockout impaired both HR repair and SSA repair efficiency (Fig. 4E, F). In addition, to exclude an indirect effect of ARID1A depletion on gene transcription regulation, we examined the key molecules involved in DDR and DSB end resection in ARID1A-depleted cells and observed no

apparent reduction in protein levels (Supplementary Fig. 9 and 10). Together, these data suggested that initial DSB end resection resulting from ATM–MRN complex-dependent signaling recruits ATR in complex with ARID1A to promote DSB end resection and ATR activation and thereby augment DSB-induced DNA damage signaling.

ARID1A Deficiency Sensitizes Cells to PARP Inhibitors

Inhibitors of PARP1, an enzyme involved in repairing DNA SSBs (38, 39), are now in clinical trials and showing promising activity. PARP inhibitor treatment causes failure of SSB repair, which can lead to DSBs when DNA replication forks stall and collapse at persistent SSB lesions (38, 39). Furthermore, PARP inhibitors trap PARP on DNA eventually leading to DSBs. Therefore, PARP inhibitors are selectively lethal to cells lacking BRCA1 or BRCA2, two proteins involved in repairing DSBs, or lacking other components of the DSB break repair pathway, but exhibit minimal toxic effects on normal cells and less activity in cancer cells without DSB repair deficiency(38, 39). We found that ARID1A-depleted cells exhibited a significant G2/M checkpoint defect in response to DSBs, which may lead to insufficient cell cycle arrest to allow efficient DSB repair (Fig. 2). In addition, ARID1A deficiency impaired DSB repair through both HR and SSA mechanisms (Fig. 4). On the basis of these observations, we reasoned that ARID1A deficiency may render cells vulnerable to DSBs induced by PARP inhibitors. We tested this hypothesis in a variety of isogenic models with multiple PARP inhibitors that are currently used in clinical trials.

First, we knocked down ARID1A in two non-transformed breast epithelial cell lines, MCF10A and HMEC, and then treated the cells with PARP inhibitors olaparib, rucaparib, and veliparib. As shown in Fig. 5A, B, PARP inhibitors selectively decreased the survival of cells with decreased ARID1A expression. Next, we tested whether ARID1A depletion sensitized HCT116 colon cancer cells and MDA-MB-231 breast cancer cells to PARP inhibitors. We treated the cells with olaparib and BMN673, a potent PARP inhibitor (40, 41). Strikingly, ARID1A-knockdown cells showed remarkably reduced colony formation in the presence of PARP inhibitors (Fig. 5C and Supplementary Fig. 11A). As we observed the reduced colony formation in ARID1A-deficient HCT116 cells compared to control cells, we further examined the growth rate of these cells. As shown in Supplementary Fig. 11B, ARID1A knockdown reduced cell growth. However we did not observe cytotoxic effects of ARID1A knockdown alone. It is noteworthy that not only the number of colonies but also the average colony size was lower with BMN673 than with olaparib in ARID1A knockout cells, suggesting that BMN673 strongly inhibits cancer cell survival. In line with these findings, significantly enhanced apoptosis after exposure to PARP inhibitors was observed in ARID1A-depleted MDA-MB-231 cells (Fig. 5D, E), HCT116 cells (Fig. 5F) and HOC8 ovarian cancer cells (Supplementary Fig. 12). To confirm that ARID1A deficiency sensitizes cells to PARP inhibitors, we conducted four sets of experiments. Firstly, we examined the correlation between ARID1A expression and PARP inhibitor sensitivity in a collection of ovarian cancer cells. As shown in Supplementary Fig. 13A-D, sensitivity to BMN673 was associated with ARID1A protein levels. Secondly, we reconstituted ARID1A-knockout HCT116 cells and ARID1A-knockdown U2OS cells with wild-type ARID1A. As shown in Supplementary Fig. 14A and B, wild-type ARID1A significantly reduced PARP-inhibitor-

induced apoptosis. In the third experiment, we reconstituted ARID1A-knockout HCT116 cells with deletion mutants, which lack the ATR interaction domain and are not recruited to DSBs. In contrast to wild-type ARID1A, these deletion mutants did not rescue the apoptosis induced by PARP inhibitors in ARID1A-depleted cells (Fig. 5G and Supplementary Fig. 14C). This result suggested that the role of ARID1A in DSB repair contributes to cellular sensitivity to PARP inhibitor treatment. In the fourth experiment, we reconstituted patient-derived mutations of ARID1A in HCT116 knockout cells (Supplementary Fig. 14D). We found that two frame-shift mutations (c5715delA and c5548delG) reduced protein expression and failed to rescue PARP inhibitor-induced apoptosis. In addition, a missense mutation (cA5337), which is localized in the ARID1A-ATR interaction region, was unable to rescue apoptosis induced by BMN673. In contrast, another missense mutation (cC6693T), which is localized outside the interaction region, partially rescued apoptosis. Furthermore, we determined whether ARID1A-deficient cells are sensitive to PARP inhibitors because of defective ATR signaling. To this end, we treated wild-type cells and ARID1A knockdown cells with a selective ATR inhibitor (Supplementary Fig. 15). We found that ATR inhibitor treatment significantly increased BMN673-induced apoptosis in wild type cells, which showed even a stronger effect than ARID1A knockdown, suggesting ARID1A deficiency only partially inhibits the function of ATR. Moreover, ARID1A knockdown did not significantly increased PARP inhibitor sensitivity in ATR inhibitor treated cells suggesting that the major effect of ARID1A loss is mediated by defective ATR function. These results showed that ATR inhibition of wild-type cells confers sensitivity to PARP inhibitors, which is epistatic with ARID1A deficiency. Collectively, these data further demonstrated that ARID1A deficiency sensitizes cancer cells to PARP inhibition potentially through inhibition of ATR function in DSB repair.

Compared to olaparib and veliparib, rucaparib and BMN673 at the same concentration showed stronger effects on cell survival and apoptosis in ARID1A-deficient cells (Fig. 5E, F). Whether this represents differential activity on PARP inhibition or trapping or EC50 values for the enzyme in intact cells remains to be determined. Based on the increased activity, we examined the dose-dependence of rucaparib- and BMN673-induced apoptosis in ARID1A-depleted cells. As shown in Fig. 5H, both drugs induced a stronger apoptotic effect in ARID1A-depleted cells than in control cells. Consistent with the EC50 for PARP inhibition in intact cells (40, 41), BMN673 induced apoptosis at much lower concentrations than rucaparib in ARID1A deficient cells. Therefore, in the next step, we tested the antitumor effects of BMN673 against ARID1A-deficient cancer cells i*n vivo*.

PARP Inhibitor BMN673 Selectively Inhibits ARID1A-Deficient Tumors in Xenograft Models

We treated nude mice bearing ARID1A-deficient and parental MDA-MB-231 breast cancer tumor and ARID1A-depleted and parental HCT116 colon cancer tumors in the opposite flanks with and without oral 0.33 mg/kg BMN673 daily. Because of the significant tumor burden in the untreated group, HCT116 xenograft mice were only treated with BMN673 for 16 days. After 1 week of treatment, a selective antitumor efficacy of BMN673 was observed in ARID1A-depleted HCT116 cells, and this antitumor effect was more marked at treatment day 16 (Fig. 6A, B). In contrast, BMN673 was without effect in mice bearing parental HCT116 cells (Fig. 6C). MDA-MB-231 xenografts, which grew more slowly, were treated

with BMN673 for 30 days. Once again BMN673 significantly inhibited tumor growth in ARID1A-deficient cancer cells but not wild type cells (Fig. 6A, D and E). Thus in both xenograft models, growth of ARID1A-deficient xenografts was suppressed by BMN673 compared to vehicle (Fig. 6F), but growth of ARID1A-wild-type xenografts was not (Fig. 6F).

We analyzed the expression of the DDR marker phosphorylated CHK1 and the apoptosis marker cleaved caspase 3 in xenograft tumor tissues. As expected, in response to BMN673, ARID1A-deficient cancer cells exhibited much lower expression of p-CHK1 than did control cells with wild-type ARID1A (Fig. 6G) consistent with loss of ARID1A decreasing the DDR induced by BMN673. Furthermore, ARID1A-deficient tumor cells exhibited enhanced apoptosis after BMN673 treatment (Fig. 6G). Taken together, our data suggest that targeting the defective DDR that occurs in ARID1A-deficient cells with PARP inhibitors could be beneficial for cancer patients with ARID1A-deficient tumors.

DISCUSSION

As shown in the proposed model (Supplementary Fig. 16), our study indicates that ARID1A interacts with ATR, is recruited to sites of DNA damage in an ATR-dependent manner and facilitates and/or accelerates effective DNA DSB end resection. This ARID1A-mediated chromatin remodeling, by promoting efficient DSB end resection, is required for sustaining ATR-dependent signaling from DSBs and repair of DSBs through HR pathways. Our *in vitro* and *in vivo* data further show that PARP inhibitors demonstrate selective activity against ARID1A-deficient cells. Collectively, our results provide mechanistic insights into how ARID1A suppresses tumorigenesis and therapeutic liabilities engendered by ARID1A deficiency could be exploited clinically.

In the DNA damage signaling network, similar regulatory mechanisms are used for promoting/sustaining cellular responses to DNA damage. For example, when DSBs occur, ATM and/or ATR phosphorylate histone H2A variant H2AX, which can spread thousands of base pairs around DSB sites (42, 43). The presence of phosphorylated H2AX (γ-H2AX) provides docking sites to recruit DNA damage-responsive sensors such as NBS1 and MDC1, and recruitment of these sensor proteins further activates or maintains ATM kinase activity (phosphorylation of H2AX) and amplifies ATM signaling (44-46). Processing of DSB ends to single-strand ends is required for ATR activation. The initial activation of ATR, which is dependent on MRN complex–ATM signaling, may not require ARID1A. Consistent with this recruitment-amplification/sustaining model, our data showed that ARID1A is recruited to DSBs via its interaction with ATR and thereby helps sustain ATR activation via promoting resection.

It is worth noting that our data showed that ARID1A deficiency reduced ATR activation in response to IR-induced DSBs. However, no significant change of ATR activation in response to HU was observed in ARID1A-deficient cells as examined in our current experimental condition. There are two possible explanations for this observation. First, the different structures of DSBs caused by IR and HU may be associated with distinct mechanisms of ATR activation. Whereas IR induces DSBs with blunt ends, HU induces

replication stress-associated DSBs in S phase (47). These types of DSBs occur at stalled/collapsed replication forks, which normally are one-ended and associated with replication fork structure. We speculate that in response to IR-induced DSBs, chromatin remodeling activity mediated by ARID1A is required to promote efficient DSB end resection to sustain ATR signaling. However, in response to HU-induced (replication stress-associated, one-end) DSBs, ARID1A-mediated chromatin remodeling may not be required to promote ATR activation given the relatively open chromatin structure of replication forks during DNA replication in S phase. If the chromatin remodeling activity is required, it is likely that a different chromatin remodeling mechanism independent of ARID1A is involved in HU-induced one-end DSBs. Second, although HU induces replication stress-associated DSBs, HU primarily induces extensive formation of single-strand DNA coated with RPA. This DNA structure provides a molecular basis for activating ATR through ATRIP and TOPBP1 in S phase, which does not require DNA end resection. Thus, on the basis of our data, we speculate that ARID1A does not play a determinative role in regulating HU-induced ATR activation.

Multiple studies have indicated tumor suppressor roles for ARID1A in transcriptionally regulating cell cycle progression (48-50). Interestingly, our study shows that ARID1A directly regulates the DNA damage checkpoint independent of its roles in transcriptionally regulating cell cycle progression. Consistent with this caretaker role of ARID1A, previous studies found that knockdown of SWI/SNF core component BRG1 or BRM could affect DNA repair pathways and proper mitosis segregation (1, 51). Consistent with this contention, a recent study reported that SWI/SNF factors are required for cellular resistance to DNA damage (52). To understand detailed mechanisms of how ARID1A regulates ATR activation in response to DSBs, two additional questions are of critical importance. Firstly, is the role of ARID1A in regulating the function of the SWI/SNF complex related to its effects on ATR function? Our data suggest that the SWI/SNF complex is required for maintaining checkpoint activation. It is likely that ARID1A is required for recruiting or stabilizing the SWI/SNF complex at DSBs. Whether, there are functionally restricted ARID1A/SWI/SNF complex independently involved in DNA damage repair or transcriptional regulation or whether the same protein complexes can mediate both processes depending on the cellular context will be important to ascertain. Secondly, how do patient-derived mutations of ARID1A affect its function in DNA damage response? A variety of mutations are found in ARID1A in human cancers. Many of the mutations result in mutation mediated RNA decay and unstable protein, but a number of the mutant ARID1A proteins are expressed. Thus to functionalize patient-derived mutations is not only important for understanding the molecular mechanisms of ARID1A in DNA damage response, but also important for stratifying patients for clinical trials of targeted therapy with PARP inhibitors.

Our results showed that ARID1A deficiency impairs DSB repair, which normally should delay the progression of cell cycle in order to allow resolution of the DSBs. However we observed that ARID1A-deficient cells progress more quickly through the cell cycle, suggesting the role of ARID1A in the ATR-mediated DNA damage checkpoint plays a dominant role in determining cell cycle progression after DNA damage. It is likely that impaired DSB repair and cell cycle checkpoint activity may allow ARID1A-deficient cells to transmit damaged (unrepaired) DNA to the next cell cycle, which could potentially lead to

genomic instability. As suggested by a recent study in gastric cancer, ARID1A mutations are associated with increased microsatellite instability (MSI), it is of interest to investigate whether ARID1A deficiency promotes the mutational process in tumorigenesis or whether ARID1A is a target for MSI.

PARP inhibitor monotherapy is well tolerated in patients but has minimal therapeutic effects in the absence of specific genetic defects such as *BRCA1/BRCA2* mutations (53). Thus, our study provides a mechanistic rationale for testing the efficacy of PARP inhibitors in ARID1A-deficient tumors either along or in combination. However as noted above, not all *ARID1A* mutations are demonstrated to compromise DDR. Therefore, it is imperative to select ARID1A-mutant tumors for PARP inhibitor treatment on the basis of the biological significance of their specific mutations.

Specific inactivating mutations in several other SWI/SNF subunits, including PBRM1, ARID2, ARID1B, BRG1, SNF5, and BRD7, have also been frequently found in human cancers (1). However, mutations in different SWI/SNF subunits lead to distinct cancer spectrums (1). In addition, mouse models with genetic knockout of different SWI/SNF subunits exhibit distinct phenotypes (1, 54). These findings suggest that individual subunits may have distinct tumor suppressor roles in specific tissue contexts. Given the diverse combinations and interactions of subunits in a particular SWI/SNF, it is possible that ARID1A has distinct effects on tumorigenesis in different tissues. Therefore, the mechanisms by which ARID1A exerts its tumor suppressor function may be tissue dependent. The answer to this question will be instrumental to guide therapy with DNA-damage-inducing agents such as PARP inhibitors. In the current study, we used well-established cancer cell models, HOC8, HCT116 and MDA-MB-231, and normal diploid epithelial cell models, MCF10A and HMEC, as representative model systems to test our hypothesis. Thus, it is necessary to confirm our findings in additional cancer models such as ovarian clear cell carcinoma models, which exhibit the highest ARID1A mutation rate among all cancer types. It has been found that *ARID1A* mutations cooperate with activation of the PI3K/AKT pathway in promoting tumorigenesis (2, 3). A recent study showed that depletion of ARID1B reduces survival of ARID1A-mutant cancer cells (55). Thus, PARP inhibitors in combination with PI3K/AKT inhibitors or strategies targeting ARID1B may provide new therapeutic avenues for patients with ARID1A-mutant tumors.

METHODS

Cell Culture and Plasmids

HCT116 parental and ARID1A knockout (Q456*/Q456*) cell lines were purchased from Horizon Discovery Ltd and maintained according to the manufacturer's instructions. U2OS cells, MCF10A, HMEC and breast cancer cell line MDA-MB-231 were purchased from American Type Culture Collection. Cell lines were validated by STR DNA fingerprinting using the AmpF_STR Identifiler kit according to manufacturer instructions (Applied Biosystems cat 4322288). The STR profiles were compared to known ATCC fingerprints, to the Cell Line Integrated Molecular Authentication database (CLIMA) version 0.1.200808 (Nucleic Acids Research 37:D925-D932 PMCID: PMC2686526 and to the MD Anderson fingerprint database. The STR profiles matched known DNA fingerprints or were unique.

The U2OS cell lines were obtained from ATCC in 2013. The authentication of the breast cancer cell lines and ovarian cancer cell lines was performed in the MDACC Characterized Cell Line Core facility in 2012 and 2013. HCT116 and ARID1A knockout cell lines were obtained from Horizon Discovery, Inc at the end of 2012 and automatically replaced by the new batch of cell line every year since then through the contract with the company. U2OS cells were maintained in McCoy's 5A medium (Cellgro) supplemented with 10% FBS with glutamine, penicillin, and streptomycin. MDA-MB-231 breast cancer cells were grown in RPMI 1640 medium supplemented with 10% FBS. HMEC were grown in HuMEC medium with growth supplement. MCF10A cells were maintained in mammary epithelial growth medium (Clonetics), a proprietary serum-free medium containing insulin, hydrocortisone, epidermal growth factor, and bovine pituitary extract. Cells were incubated at 37°C in a humidified incubator with 5% CO_2.

The pCDNA6-V5-ARID1A and its deletion forms 1-1758aa and 1759-2285aa were kindly provided by Dr. Ie-Ming Shih, Johns Hopkins University School of Medicine. The EGFP-ARID1A and its mutant forms were generated by Custom DNA Constructs. Other mutations were generated by QuickChange II Site-Directed Mutagenesis Kit (Stratagene). The identity of all plasmids was confirmed by sequencing at the MD Anderson Cancer Center Sequencing and Microarray Facility.

Antibodies and Reagents

Anti-ARID1A (1:500) and anti-RPA (1:1,00) antibodies were purchased from Bethyl Laboratories. Anti-V5 (1:1,000) was purchase from Life Technology. Anti-γ-H2AX (1:1,000) was purchased from Millipore. Anti-53BP1 (1:2,000) was purchased from Novus Biologicals. Anti-ATR (1:500) was purchase from Santa Cruz Biotechnology. Anti-ATRIP (1:1,000), p-ATM (1:500), p-Chk1 (1:500), p-Chk2 (1:500), GFP (1:1,000) and p-H3 (1:500) were purchased from Cell Signaling Technology. Anti-p-ATR antibody was kindly provided by Dr. Lee Zou (Massachusetts General Hospital Cancer Center, Harvard Medical School) Anti-Tubulin and anti-β-Actin were purchased from Sigma. Apoptosis detection kit was purchased from BD Biosciences. PARP inhibitors olaparib, veliparib, rucaparib, and BMN673 were purchased from Selleckchem. The silver staining kit was purchased from Thermo Scientific.

RNA Interference

ARID1A knockdown was achieved by RNA interference using a lentiviral vector-based MISSION shRNA or siRNA (Sigma). Lentiviral particles corresponding to the MISSION shRNA ARID1A- NM_006015 target set were used, as well as a MISSION nontarget shRNA control. The shRNA sequences were: V3LHS 410041 (#1), TAAATAGCTGTGTCTCGCT; V2LHS_71866 (#2), TCTTGAGATAGCTCCTGCG. Specificity and efficacy of the shRNA ARID1A procedure were evaluated by Western blotting after transduction and puromycin selection in cells. siRNA transfection was conducted using oligofectamine (Life Technology) according to the manufacturer's instructions.

Immunoblotting, IP, and Chromatin Fractionation

Cells were washed in PBS, and cellular proteins were extracted in 8-M urea lysis buffer plus protease and phosphatase inhibitors (GenDEPOT) for 30 min at 4°C. Lysates were cleared by centrifugation, and proteins were separated by gel electrophoresis. Membranes were blocked in PBS-0.1% Tween 20 (PBS-T)/5% (w/v) milk for 1 h at room temperature. Membranes were then incubated with primary antibodies diluted in PBS-T/5% (w/v) milk at 4°C overnight. Subsequently, membranes were washed with PBS-T and incubated with horseradish peroxidase secondary antibody (1:2,000) (Jackson ImmunoResearch) diluted in PBS-T/5% skim milk. Membranes were washed in PBS-T, and bound antibody was detected by enhanced chemiluminescence (GE Healthcare). IP was performed by incubating lysates from 6×10^6 cells with 1 μg of antibody at 4°C overnight, followed by addition of 20 μL of protein A/G-conjugated agarose beads (GE Healthcare). The precipitates were washed four times with ice-cold PBS, resuspended in 6× Laemmli buffer, and resolved by SDS-PAGE followed by immunoblotting. The preparation of chromatin fractions and Western blot analyses, including the conditions for RPA analysis, were performed as described previously (21, 56).

HR and SSA Repair Assays

SSA assay cells were kindly provided by Dr. Stark (Beckman Research Institute of the City of Hope). The HR and SSA repair assays were performed as described previously (21, 57-60).

Immunofluorescent Staining for Foci Formation

For detection of DNA damage-induced foci of γ-H2AX, 53BP1, and p-RPA32, immunofluorescent staining was performed essentially as described previously (21, 56). After treatment, cells were firstly subjected to cytoskeleton extraction/stripping (cytoskeleton buffer: 10 mM PIPES pH6.8; 100 mM NaCl; 300 mM Sucrose; 3 mM MgCl2; 1 M EGTA; 0.5% Triton-X 100; stripping buffer: 10 mM Tris-HCl pH7.4; 10 mM NaCl; 3 mM MgCl2; 1% Tween 20; 0.25% Sodium Deoxychalate) to remove the unbound proteins and secondly fixed in PBS-buffered 4% paraformaldehyde. Primary antibodies were incubated at 4°C overnight and secondary antibody Alexa 488-conjugated goat anti-rabbit IgG was incubated for 1 h at room temperature. Slides were mounted in medium containing DAPI (Vector Laboratories) and analyzed under a fluorescence microscope. At least 50 cells per sample were scored, and foci were counted. Although currently available ARID1A antibodies are suitable for Western blot analysis and general fluorescent staining, they failed to detect formation of ionizing radiation (IR)-induced foci of ARID1A at DNA breaks.

ChIP Assay

DSBs were induced in cells transfected with control siRNA or ATR siRNA by I-*Sce*I expression. At indicated time points, cells were cross-linked with formaldehyde, and ChIP assays were performed with an EZ ChIP kit (Upstate) according to the manufacturer's instructions. Cellular lysates were subjected to five sets of sonication on wet ice with a 60 Sonic Dismembrator (Fisher Scientific). Each set consisted of 8 s of sonication separated by 1-min intervals on ice. ARID1A and V5 antibodies (5 μL/reaction) were used for IP. The

ChIP primers used to analyze proteins binding at DSBs were primer 1, 5′-TACGGCAAGCTGACCCTGAA-3′ (sense) and 5′-GCCCATATATGGAGTTCCGC-3′ (antisense); primer 2, 5′- GCCCATATATGGAGTTCCGC -3′ (sense) and 5′-GCCCATATATGGAGTTCCGC -3′ (antisense); primer 3, 5′-CAGGCAACTCTGCTCACTCA -3′ (sense) and 5′- GGCTATTGCTATAGGGTCCG -3′ (antisense); primer 4, 5′- GAGGCACCTGGAGCTGAG -3′ (sense) and 5′-GCTGAACTTGTGGCCGTTTA -3′ (antisense); primer 5, 5′-GAGAAAGGTGCCGAAGAAGC-3′ (sense) and 5′-GTAGCAGATGGGGCAGGTG-3′ (antisense).

Tumor Growth in Nude Mice

Male athymic nu/nu mice (6-8 weeks old) were used for all in vivo xenograft studies. Mice were quarantined for at least 1 week before experiments. All animal studies were conducted in compliance with protocols approved by the MD Anderson Cancer Center Institutional Animal Care and Use Committee. Exponentially growing MDA-MB-231 (1×10^6) or HCT116 (2×10^6) cells were implanted subcutaneously at the flank of nude mice (Left: control cells, Right: ARID1A-deficient cells). Mice were treated with vehicle or BMN673 (0.33 mg/kg) once daily by oral gavage. Tumors were measured every 2 days by caliper to determine tumor volume using the formula $[\text{length}/2]\times[\text{width}^2]$. Each cell line was tested in six different animals. For immunohistochemistry, tumor tissue samples were fixed in 4% buffered paraformaldehyde and processed for histopathologic evaluation by paraffin embedding and antibody staining.

Methods for the following assays are available in Supplementary Information: KillerRed System, Flow Cytometric Analyses, Comet assay, Colony-forming assay and Tet-On expression of ARID1A.

Statistical Analysis

All statistical analyses were performed with a two-tailed Student's *t*-test.

Supplementary Material

Refer to Web version on PubMed Central for supplementary material.

ACKNOWLEDGEMENTS

We thank Dr. Shiaw-Yih Lin (MD Anderson Cancer Center) and Dr. Grzegorz Ira (Baylor College of Medicine) for scientific discussions; Dr. Jeremy Stark (Beckman Research Institute of the City of Hope) and Dr. Lee Zou (Massachusetts General Hospital Cancer Center, Harvard Medical School) for reagents; S. Deming for proofreading the manuscript.

This work was supported in part by Cancer Center Support Grant CA016672 from the National Cancer Institute (NCI); NCI Ovarian SPORE (MDACC) Career Development Award to G.P.; NCI grant R00 CA149186 to G.P.; P50 CA098258 and P50 CA083639 to G. B. M.; Adelson Medical Research Foundation (00000205 and 00000196) to G. B. M.

G.B. Mills has received commercial research support from GlaxoSmithKline and AstraZeneca; has ownership interest in Catena Pharmaceuticals, PTV Ventures, and Spindle Top Ventures; and is aconsultant/advisory board member of AstraZeneca, Blend, Critical Outcome Technologies, HanAl Bio Korea, Illumina, Nuevolution, Pfizer, Provista Diagnostics, Roche, Signalchem Lifesciences, Symphogen, and Tau Therapeutics.

REFERENCES

1. Wilson BG, Roberts CW. SWI/SNF nucleosome remodellers and cancer. Nat Rev Cancer. 2011; 11:481–92. [PubMed: 21654818]
2. Wu JN, Roberts CW. ARID1A Mutations in Cancer: Another Epigenetic Tumor Suppressor? Cancer Discov. 2013; 3:35–43. [PubMed: 23208470]
3. Wu RC, Wang TL, Shih IM. The emerging roles of ARID1A in tumor suppression. Cancer Biol Ther. 2014; 15
4. Wang X, Nagl NG Jr. Flowers S, Zweitzig D, Dallas PB, Moran E. Expression of p270 (ARID1A), a component of human SWI/SNF complexes, in human tumors. Int J Cancer. 2004; 112:636. [PubMed: 15382044]
5. Wang X, Nagl NG, Wilsker D, Van Scoy M, Pacchione S, Yaciuk P, et al. Two related ARID family proteins are alternative subunits of human SWI/SNF complexes. Biochem J. 2004; 383:319–25. [PubMed: 15170388]
6. Wang GG, Allis CD, Chi P. Chromatin remodeling and cancer, Part II: ATP-dependent chromatin remodeling. Trends Mol Med. 2007; 13:373–80. [PubMed: 17822959]
7. Imbalzano AN, Kwon H, Green MR, Kingston RE. Facilitated binding of TATA-binding protein to nucleosomal DNA. Nature. 1994; 370:481–5. [PubMed: 8047170]
8. Kwon H, Imbalzano AN, Khavari PA, Kingston RE, Green MR. Nucleosome disruption and enhancement of activator binding by a human SW1/SNF complex. Nature. 1994; 370:477–81. [PubMed: 8047169]
9. Ciccia A, Elledge SJ. The DNA damage response: making it safe to play with knives. Mol Cell. 2010; 40:179–204. [PubMed: 20965415]
10. Jackson SP, Bartek J. The DNA-damage response in human biology and disease. Nature. 2009; 461:1071–8. [PubMed: 19847258]
11. Harper JW, Elledge SJ. The DNA damage response: ten years after. Mol Cell. 2007; 28:739–45. [PubMed: 18082599]
12. Zhou BB, Elledge SJ. The DNA damage response: putting checkpoints in perspective. Nature. 2000; 408:433–9. [PubMed: 11100718]
13. Jazayeri A, Falck J, Lukas C, Bartek J, Smith GC, Lukas J, et al. ATM- and cell cycle-dependent regulation of ATR in response to DNA double-strand breaks. Nat Cell Biol. 2006; 8:37–45. [PubMed: 16327781]
14. Myers JS, Cortez D. Rapid activation of ATR by ionizing radiation requires ATM and Mre11. J Biol Chem. 2006; 281:9346–50. [PubMed: 16431910]
15. Adams KE, Medhurst AL, Dart DA, Lakin ND. Recruitment of ATR to sites of ionising radiation-induced DNA damage requires ATM and components of the MRN protein complex. Oncogene. 2006; 25:3894–904. [PubMed: 16474843]
16. Brown EJ, Baltimore D. ATR disruption leads to chromosomal fragmentation and early embryonic lethality. Genes Dev. 2000; 14:397–402. [PubMed: 10691732]
17. Cimprich KA, Cortez D. ATR: an essential regulator of genome integrity. Nat Rev Mol Cell Biol. 2008; 9:616–27. [PubMed: 18594563]
18. Cortez D, Guntuku S, Qin J, Elledge SJ. ATR and ATRIP: partners in checkpoint signaling. Science. 2001; 294:1713–6. [PubMed: 11721054]
19. Brown EJ. The ATR-independent DNA replication checkpoint. Cell Cycle. 2003; 2:188–9. [PubMed: 12734420]
20. Vogelstein B, Papadopoulos N, Velculescu VE, Zhou S, Diaz LA Jr. Kinzler KW. Cancer genome landscapes. Science. 2013; 339:1546–58. [PubMed: 23539594]
21. Peng G, Yim EK, Dai H, Jackson AP, Burgt I, Pan MR, et al. BRIT1/MCPH1 links chromatin remodelling to DNA damage response. Nat Cell Biol. 2009; 11:865–72. [PubMed: 19525936]
22. Pierce AJ, Johnson RD, Thompson LH, Jasin M. XRCC3 promotes homology-directed repair of DNA damage in mammalian cells. Genes Dev. 1999; 13:2633–8. [PubMed: 10541549]

23. Lan L, Nakajima S, Wei L, Sun L, Hsieh CL, Sobol RW, et al. Novel method for site-specific induction of oxidative DNA damage reveals differences in recruitment of repair proteins to heterochromatin and euchromatin. Nucleic Acids Res. 2014; 42:2330–45. [PubMed: 24293652]
24. Lan L, Ui A, Nakajima S, Hatakeyama K, Hoshi M, Watanabe R, et al. The ACF1 complex is required for DNA double-strand break repair in human cells. Mol Cell. 2010; 40:976–87. [PubMed: 21172662]
25. Carpentier P, Violot S, Blanchoin L, Bourgeois D. Structural basis for the phototoxicity of the fluorescent protein KillerRed. FEBS Lett. 2009; 583:2839–42. [PubMed: 19646983]
26. Pletnev S, Gurskaya NG, Pletneva NV, Lukyanov KA, Chudakov DM, Martynov VI, et al. Structural basis for phototoxicity of the genetically encoded photosensitizer KillerRed. J Biol Chem. 2009; 284:32028–39. [PubMed: 19737938]
27. Kozlov SV, Graham ME, Peng C, Chen P, Robinson PJ, Lavin MF. Involvement of novel autophosphorylation sites in ATM activation. EMBO J. 2006; 25:3504–14. [PubMed: 16858402]
28. Nam EA, Zhao R, Glick GG, Bansbach CE, Friedman DB, Cortez D. Thr-1989 phosphorylation is a marker of active ataxia telangiectasia-mutated and Rad3-related (ATR) kinase. J Biol Chem. 2011; 286:28707–14. [PubMed: 21705319]
29. Liu S, Shiotani B, Lahiri M, Marechal A, Tse A, Leung CC, et al. ATR autophosphorylation as a molecular switch for checkpoint activation. Mol Cell. 2011; 43:192–202. [PubMed: 21777809]
30. Wang H, Wang M, Bocker W, Iliakis G. Complex H2AX phosphorylation patterns by multiple kinases including ATM and DNA-PK in human cells exposed to ionizing radiation and treated with kinase inhibitors. J Cell Physiol. 2005; 202:492–502. [PubMed: 15389585]
31. Podhorecka M, Skladanowski A, Bozko P. H2AX Phosphorylation: Its Role in DNA Damage Response and Cancer Therapy. J Nucleic Acids. 2010; 2010
32. Panier S, Boulton SJ. Double-strand break repair: 53BP1 comes into focus. Nat Rev Mol Cell Biol. 2014; 15:7–18. [PubMed: 24326623]
33. Berkovich E, Monnat RJ Jr. Kastan MB. Roles of ATM and NBS1 in chromatin structure modulation and DNA double-strand break repair. Nat Cell Biol. 2007; 9:683–90. [PubMed: 17486112]
34. Falck J, Coates J, Jackson SP. Conserved modes of recruitment of ATM, ATR and DNA-PKcs to sites of DNA damage. Nature. 2005; 434:605–11. [PubMed: 15758953]
35. Lee JH, Paull TT. ATM activation by DNA double-strand breaks through the Mre11-Rad50-Nbs1 complex. Science. 2005; 308:551–4. [PubMed: 15790808]
36. Zou L, Elledge SJ. Sensing DNA damage through ATRIP recognition of RPA-ssDNA complexes. Science. 2003; 300:1542–8. [PubMed: 12791985]
37. Polo SE, Blackford AN, Chapman JR, Baskcomb L, Gravel S, Rusch A, et al. Regulation of DNA-end resection by hnRNPU-like proteins promotes DNA double-strand break signaling and repair. Mol Cell. 2012; 45:505–16. [PubMed: 22365830]
38. Farmer H, McCabe N, Lord CJ, Tutt AN, Johnson DA, Richardson TB, et al. Targeting the DNA repair defect in BRCA mutant cells as a therapeutic strategy. Nature. 2005; 434:917–21. [PubMed: 15829967]
39. Bryant HE, Schultz N, Thomas HD, Parker KM, Flower D, Lopez E, et al. Specific killing of BRCA2-deficient tumours with inhibitors of poly(ADP-ribose) polymerase. Nature. 2005; 434:913–7. [PubMed: 15829966]
40. Cardnell RJ, Feng Y, Diao L, Fan YH, Masrorpour F, Wang J, et al. Proteomic markers of DNA repair and PI3K pathway activation predict response to the PARP inhibitor BMN 673 in small cell lung cancer. Clin Cancer Res. 2013; 19:6322–8. [PubMed: 24077350]
41. Shen Y, Rehman FL, Feng Y, Boshuizen J, Bajrami I, Elliott R, et al. BMN 673, a novel and highly potent PARP1/2 inhibitor for the treatment of human cancers with DNA repair deficiency. Clin Cancer Res. 2013; 19:5003–15. [PubMed: 23881923]
42. Bakkenist CJ, Kastan MB. DNA damage activates ATM through intermolecular autophosphorylation and dimer dissociation. Nature. 2003; 421:499–506. [PubMed: 12556884]
43. Rogakou EP, Boon C, Redon C, Bonner WM. Megabase chromatin domains involved in DNA double-strand breaks in vivo. J Cell Biol. 1999; 146:905–16. [PubMed: 10477747]

44. Lou Z, Minter-Dykhouse K, Franco S, Gostissa M, Rivera MA, Celeste A, et al. MDC1 maintains genomic stability by participating in the amplification of ATM-dependent DNA damage signals. Mol Cell. 2006; 21:187–200. [PubMed: 16427009]
45. Melander F, Bekker-Jensen S, Falck J, Bartek J, Mailand N, Lukas J. Phosphorylation of SDT repeats in the MDC1 N terminus triggers retention of NBS1 at the DNA damage-modified chromatin. J Cell Biol. 2008; 181:213–26. [PubMed: 18411307]
46. Stewart GS, Wang B, Bignell CR, Taylor AM, Elledge SJ. MDC1 is a mediator of the mammalian DNA damage checkpoint. Nature. 2003; 421:961–6. [PubMed: 12607005]
47. Ward IM, Chen J. Histone H2AX is phosphorylated in an ATR-dependent manner in response to replicational stress. J Biol Chem. 2001; 276:47759–62. [PubMed: 11673449]
48. Guan B, Wang TL, Shih Ie M. ARID1A, a factor that promotes formation of SWI/SNF-mediated chromatin remodeling, is a tumor suppressor in gynecologic cancers. Cancer Res. 2011; 71:6718–27. [PubMed: 21900401]
49. Nagl NG Jr. Patsialou A, Haines DS, Dallas PB, Beck GR Jr. Moran E. The p270 (ARID1A/SMARCF1) subunit of mammalian SWI/SNF-related complexes is essential for normal cell cycle arrest. Cancer Res. 2005; 65:9236–44. [PubMed: 16230384]
50. Eroglu E, Burkard TR, Jiang Y, Saini N, Homem CC, Reichert H, et al. SWI/SNF Complex Prevents Lineage Reversion and Induces Temporal Patterning in Neural Stem Cells. Cell. 2014; 156:1259–73. [PubMed: 24630726]
51. Dykhuizen EC, Hargreaves DC, Miller EL, Cui K, Korshunov A, Kool M, et al. BAF complexes facilitate decatenation of DNA by topoisomerase IIalpha. Nature. 2013; 497:624–7. [PubMed: 23698369]
52. Watanabe R, Ui A, Kanno S, Ogiwara H, Nagase T, Kohno T, et al. SWI/SNF Factors Required for Cellular Resistance to DNA Damage Include ARID1A and ARID1B and Show Interdependent Protein Stability. Cancer Res. 2014; 74:2465–75. [PubMed: 24788099]
53. Ellisen LW. PARP inhibitors in cancer therapy: promise, progress, and puzzles. Cancer Cell. 2011; 19:165–7. [PubMed: 21316599]
54. Roberts CW, Orkin SH. The SWI/SNF complex--chromatin and cancer. Nat Rev Cancer. 2004; 4:133–42. [PubMed: 14964309]
55. Helming KC, Wang X, Wilson BG, Vazquez F, Haswell JR, Manchester HE, et al. ARID1B is a specific vulnerability in ARID1A-mutant cancers. Nat Med. 2014; 20:251–4. [PubMed: 24562383]
56. Peng G, Dai H, Zhang W, Hsieh HJ, Pan MR, Park YY, et al. Human Nuclease/helicase DNA2 Alleviates Replication Stress by Promoting DNA End Resection. Cancer Res. 2012
57. Bennardo N, Cheng A, Huang N, Stark JM. Alternative-NHEJ is a mechanistically distinct pathway of mammalian chromosome break repair. PLoS Genet. 2008; 4:e1000110. [PubMed: 18584027]
58. Wang Q, Goldstein M, Alexander P, Wakeman TP, Sun T, Feng J, et al. Rad17 recruits the MRE11-RAD50-NBS1 complex to regulate the cellular response to DNA double-strand breaks. EMBO J. 2014; 33:862–77. [PubMed: 24534091]
59. Stecklein SR, Kumaraswamy E, Behbod F, Wang W, Chaguturu V, Harlan-Williams LM, et al. BRCA1 and HSP90 cooperate in homologous and non-homologous DNA double-strand-break repair and G2/M checkpoint activation. Proc Natl Acad Sci U S A. 2012; 109:13650–5. [PubMed: 22869732]
60. Takizawa Y, Qing Y, Takaku M, Ishida T, Morozumi Y, Tsujita T, et al. GEMIN2 promotes accumulation of RAD51 at double-strand breaks in homologous recombination. Nucleic Acids Res. 2010; 38:5059–74. [PubMed: 20403813]

SIGNIFICANCE

ARID1A has been identified as one of the most frequently mutated genes across human cancers. Our data suggest that clinical utility of PARP inhibitors might be extended beyond patients with BRCA mutations to a larger group of patients with *ARID1A*-mutant tumors, which may exhibit therapeutic vulnerability to PARP inhibitors.

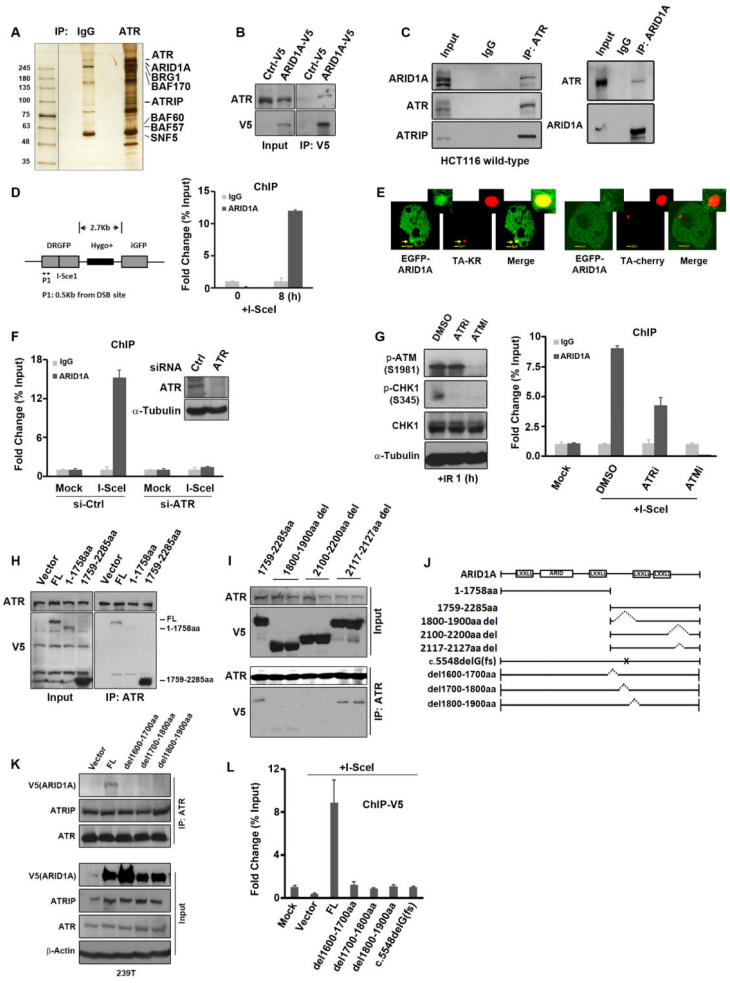

Figure 1. ARID1A interacts with ATR and is recruited to DSBs

(A) Silver staining of the ATR complex separated by SDS-PAGE. The whole-cell extracts were prepared from 293T cells. ATR-interacting proteins including ATRIP and ARID1A are indicated.

(B) Co-IP of ATR with ARID1A using anti-V5 antibody analyzed by Western blotting from 293T cells transfected with empty vector V5-control (Ctrl-V5) or V5-ARID1A.

(C) Endogenous interaction between ARID1A and ATR analyzed by reciprocal IP and Western blotting from HCT116 cells.

(D) ARID1A recruitment to I-*Sce*I-induced DSBs analyzed by ChIP assay. DRGFP construct containing a cutting site for I-*Sce*I restriction enzyme was stably integrated into U2OS cells as described in Supplementary Fig. 3 Eight hours after I-*Sce*I transfection, ChIP assay was performed. qPCR analyses were used to detect the enrichment of ARID1A relative to the IgG control (mean ± SEM; n=3).

(E) ARID1A was localized at DNA damage sites. EGFP-tagged ARID1A and TA-KR or TA-mcherry were transfected into U2OS TRE cells. The KillerRed spot was activated with 559-nm laser to induce DNA damage. Representative images after DNA damage are shown. Yellow arrowheads: DNA damage induced by a tetR-KR expression and light activation as

described in Supplementary Fig. 4. 10-20 cells/experiment and at least 50 cells in total from three independent experiments were counted to calculate the positive percentage.

(F) ATR was required for recruitment of ARID1A to DSBs. DRGFP-U2OS cells were transfected with control (Ctrl) siRNA or ATR siRNA (SMARTpool). Forty-eight hours later, cells were transfected with I-*Sce*I plasmid. CHIP assay was conducted 8 h after I-*Sce*I transfection, and qPCR analyses were used to detect the enrichment of ARID1A relative to the IgG control (mean ± SEM; n=3).

(G) Recruitment of ARID1A to DSBs was dependent on ATM/ATR signaling. DRGFP-U2OS cells were pretreated with ATR inhibitor (ATRi) VE-821 (2 μM) or ATM inhibitor (ATMi) KU55933 (10 μM) for 30 min and incubated with the inhibitors for an additional 8 h during I-*Sce*I transfection. ChIP analyses were performed 8 h after induction of DSBs by I-*Sce*I transfection. (Left) Phosphorylation of ATM/ATR substrates was detected by the indicated antibodies. (Right) qPCR analyses were used to detect the enrichment of ARID1A relative to the IgG control (mean ± SEM; n=3).

(H, I) C-terminal half of ARID1A bound to ATR. 293T cells were transfected with plasmids encoding full-length V5-ARID1A (FL) or deletion constructs of V5-ARID1A. Cell lysates were immunoprecipitated using anti-ATR antibody.

(J) Schematic diagram of ARID1A deletions and mutants.

(K) Deletion V5-ARID1A constructs were transfected into 293T cells. Cell lysates were immunoprecipitated using anti-ATR antibody, the interaction of ATR to ARID1A mutants were investigated by Western blots using anti-V5 antibody.

(L) Deletion ARID1A mutants had reduced enrichment at I-*Sce*I-induced DSBs. DRGFP-U2OS cells were transfected with wild-type or mutant V5-ARID1A. Forty-eight hours later, cells were transfected with I-*Sce*I, and 8 h later, ChIP assays were conducted with anti-V5 beads. qPCR analyses were used to detect the enrichment of ARID1A relative to the vector control (mean ± SEM; n=3; *$p<0.01$). Expression of these constructs was shown in Supplementary Fig. 5.

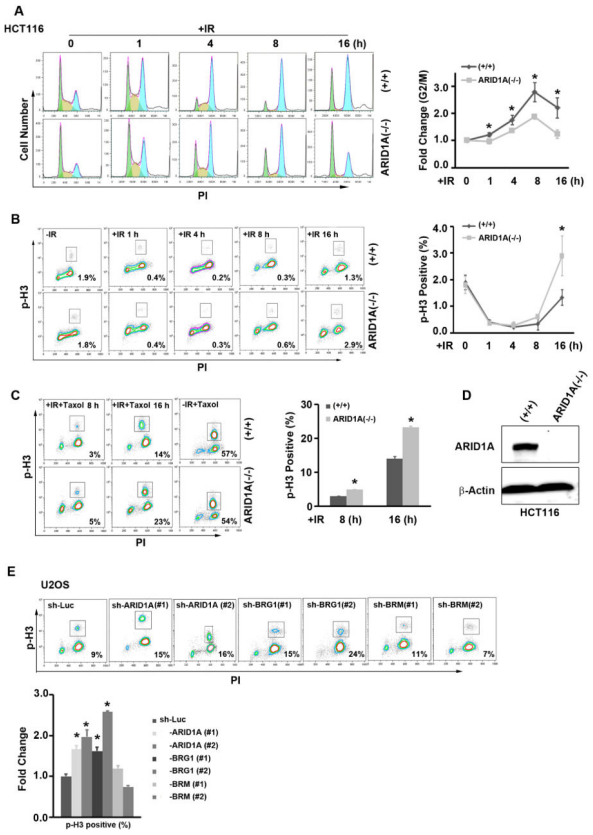

Figure 2. ARID1A deficiency impairs G2/M DNA damage checkpoint

(A, B) Control (+/+) and ARID1A-depleted (−/−) HCT116 cells were exposed to IR (7 Gy), and DNA content (A) and phosphor-Histone H3 (p-H3) (B) were determined at indicated time points after irradiation.

(C) Control cells (+/+) and ARID1A-depleted (−/−) HCT116 cells were exposed to IR (7 Gy) or left untreated and subsequently grown in the presence of paclitaxel (Taxol) (2 μM). Phosphor-Histone H3 (p-H3) was determined at the indicated time points after irradiation.

(D) Western blot analyses confirmed the effectiveness of ARID1A depletion in HCT116 ARID1A knockout cells.

(E) U2OS cells with stable knockdown of ARID1A, BRG1, or BRM with shRNAs. Phosphor-Histone H3 (p-H3) was determined 16 h after IR in the presence of paclitaxel.

(A-C, E) (Left) Representative images. (Right) Quantitative results representing the mean ± SD of three independent experiments. *p<0.05.

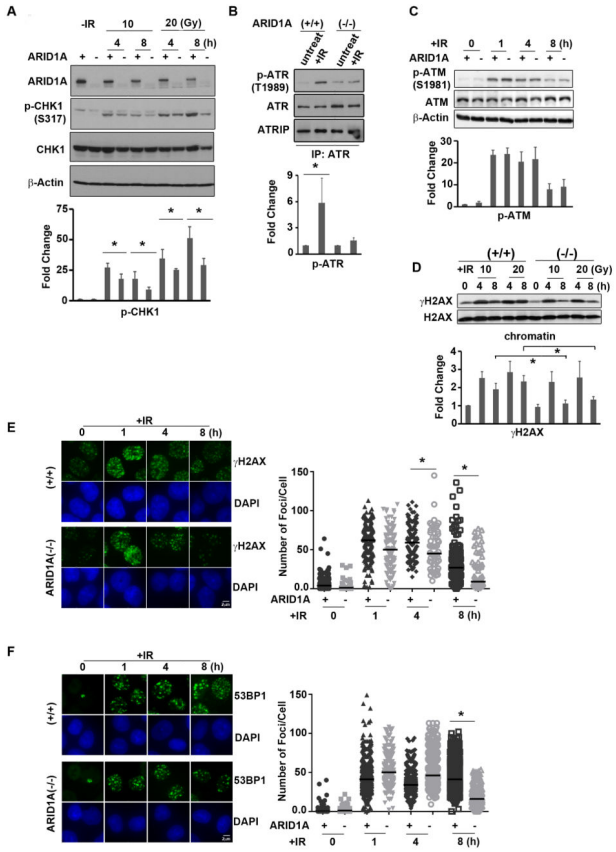

Figure 3. ARID1A is required for DSB-induced ATR activation and checkpoint signaling

(A-C) Control (+/+) and ARID1A-depleted (−/−) HCT116 cells were exposed to IR and harvested at the indicated time points. Whole cell lysates were immunoblotted with the indicated antibodies. untreat, untreated. Densitometry analyses of indicated protein values (phosphorylated protein normalized against total protein for each lane) were shown at the bottom of Western Blots (A-D). The control lane was set as 1. Each value represents the mean ± SD of three independent experiments (* P≤ 0.05).

(D) Control (+/+) and ARID1A-depleted (−/−) HCT116 cells were exposed to IR and harvested at the indicated time points. Chromatin fractionation was immunoblotted with the indicated antibodies.

(E, F) Control (+/+) and ARID1A-depleted (−/−) HCT116 cells were exposed to IR (7 Gy) and immunostained with the indicated antibodies. (Left) Representative images. Scale bar, 2 μm. (Right) Data from three independent experiments. *p<0.01.

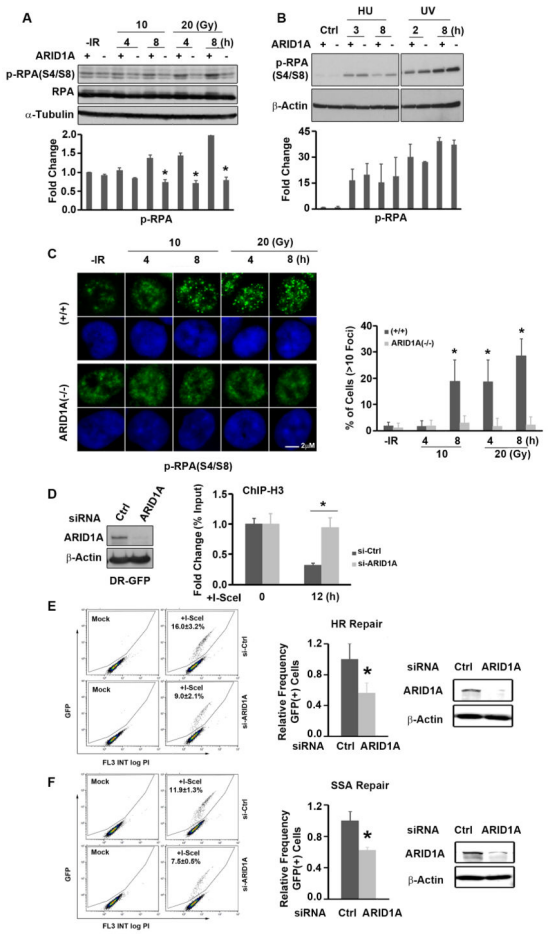

Figure 4. ARID1A promotes DSB end resection

(A, B) Western blot analysis of RPA phosphorylation [p-RPA(S4/S8)] at the indicated time points after exposure to IR (A) or replication stress stimuli (HU 2 mM and UV 50 J/m^2) (B) in control (+/+) and ARID1A-depleted (−/−) HCT116 cells. Ctrl, control. Densitometry analyses of indicated protein values (phosphorylated protein normalized against total protein for each lane) were shown at the bottom of Western Blots (A-B). The control lane was set as 1. Each value represents the mean ± SD of three independent experiments (* P≤ 0.05).

(C) Control (+/+) and ARID1A-depleted (−/−) HCT116 cells were exposed to IR and immunostained with p-RPAS4/S8. (Left) Representative images. Scale bar, 2 μM. (Right) Quantitative results represent the mean± SD of three independent experiments. *p<0.01. Representative images of multiple cells were shown in Supplementary Fig. 8B.

(D) DRGFP-U2OS cells were transfected with control siRNA or ARID1A siRNA (SMARTpool). Forty-eight hours later, cells were transfected with I-*Sce*I plasmid. ChIP assay was conducted 8 h after I-*Sce*I transfection, and qPCR analyses were used to detect the enrichment of H3 relative to the IgG control (mean ± SEM; n=3; *p<0.01). Western blot analyses to demonstrate the effective ARID1A knockdown are shown next to the graph.

(E, F) Defective HR repair (E) and SSA repair (F) in ARID1A-deficient cells upon DSB induction by I-*Sce*I. (Left) Representative flow cytometry profile. (Right) Each value is relative to the percentage of GFP-positive cells in I-*Sce*I-transfected cells without siRNA

transfection, which was set to 1 and represents the mean ± SD of three independent experiments. *p<0.01. Western blot analyses to demonstrate the effective ARID1A knockdown are shown next to the graph. Ctrl, control.

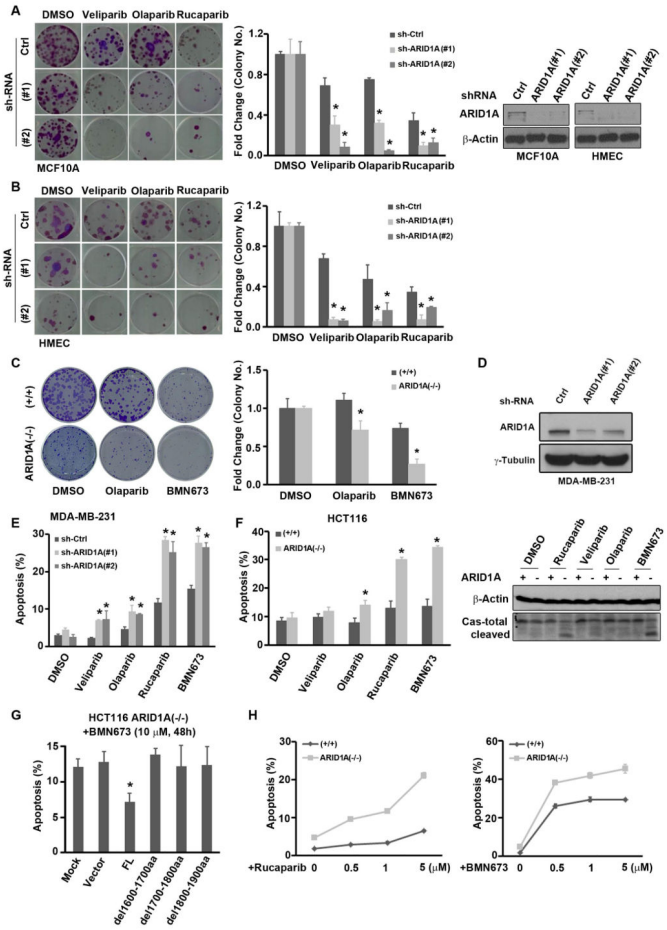

Figure 5. ARID1A deficiency sensitizes cells to PARP inhibitors

(A-C) Stable-ARID1A-knockdown nontransformed MCF10A normal breast epithelial cells (A) and HMECs (B) and ARID1A-knockout HCT116 cells (C) were treated with the indicated PARP inhibitors, each at a concentration of 10 μM. Clonogenic assay was performed. (Left) Representative images. (Right) Quantitative results represent the mean ± SD of three independent experiments. *p<0.01. Western blot analyses to demonstrate the effective ARID1A knockdown are shown next to the graphs. Ctrl, control.

(D) Western blot analyses show the effective ARID1A knockdown in MDA-MB-231 cells.

(E and F) Stable-ARID1A-knockdown MDA-MB-231 cells (E) and ARID1A-knockout HCT116 cells (F) were treated with the indicated PARP inhibitors for 72 h, and apoptosis was determined by annexin V staining. Quantitative results represent the mean ± SD of three independent experiments. *p<0.01. Western blot analyses to demonstrate the activation of Caspase-3 in ARID1A-knockout HCT116 cells are shown next to the graphs.

(G) ARID1A-knockout HCT116 cells were reconstituted with wild-type or mutant ARID1A transiently and exposed to BMN673 for 48 h. Apoptosis was determined by annexin V staining. Representative results from three independent experiments were shown (mean ± SEM). *p<0.05. Protein expression of these constructs was shown in Supplementary Fig. 14C.

(H) ARID1A-knockout HCT116 cells were exposed to rucaparib or BMN673 in a dose-dependent manner for 48 h. Apoptosis was determined by annexin V staining. Results shown are mean ± SD of three independent experiments.

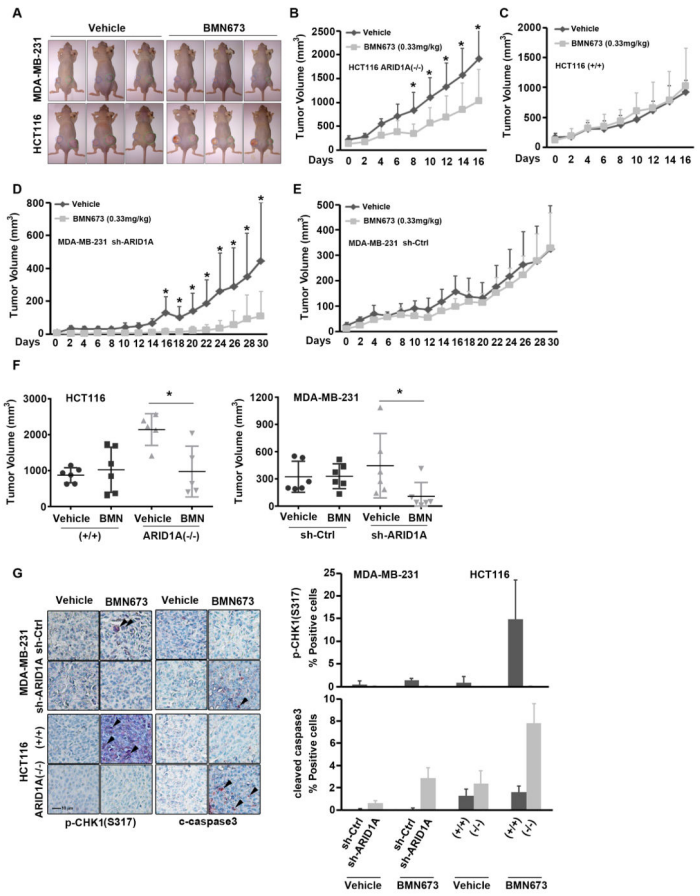

Figure 6. BMN673 selectively inhibits ARID1A-deficient xenograft tumor growth

(A) Representative images of MDA-MB-231 and HCT116 xenografts treated with vehicle control and BMN673 at the end point of scheduled treatment. (Left side-blue circle: control cells, Right side-green circle: ARID1A-deficient cells)

(B-E) Control and ARID1A-depleted HCT116 cells (B, C) and MDA-MB-231 cells (D, E) were inoculated subcutaneously in athymic nu/nu mice. Mice were randomized to vehicle control and BMN673 treatment groups. Average tumor volume was plotted against days of treatment (n=6 for each group; *p<0.01).

(F) Average tumor volume of each group was determined at the end of the scheduled treatment (n=6 for each group; *p<0.01).

(G) Representative examples of the immunohistochemistry analyses of xenograft tumors with anti-phospho-CHK1 (S317) and anti-actived caspase 3 antibodies. Scale bar, 50 μM. Quantification of anti-phospho-CHK1 (S317) and anti-actived caspase 3-positive cells of three individual tumors. *p<0.01.